Available online at www.sciencedirect.com
SCIENCE DIRECT®
Journal of Non-Crystalline Solids 336 (2004) 71–83
JOURNAL OF NON-CRYSTALLINE SOLIDS
www.elsevier.com/locate/jnoncrysol

Bubble transport in three-dimensional laminar gravity-driven flow – mathematical formulation

Laurent Pilon [a,*], Andrei G. Fedorov [b], D. Ramkrishna [c], Raymond Viskanta [d]

[a] Mechanical and Aerospace Engineering Department, University of California, Engineering IV Room 46-147C, Los Angeles, CA 90095-1597, USA
[b] G.W. Woodruff School of Mechanical Engineering, Georgia Institute of Technology, Atlanta, GA 30332-0405, USA
[c] School of Chemical Engineering, Purdue University, West Lafayette, IN 47907, USA
[d] School of Mechanical Engineering, Purdue University, West Lafayette, IN 47907, USA

Received 19 September 2003

Abstract

This paper presents a complete set of coupled equations that govern the bubble transport in three-dimensional gravity-driven flow. The model accounts for bubble growth or shrinkage due to pressure and temperature changes as well as for multiple gas diffusion in and out of the bubbles but neglects bubble coalescence, break-up, and nucleation. The model applies to glass melting furnaces but it could be extended to other two-phase flow applications such as metal and polymer processing, passive cooling systems, and two-phase flow around naval surface ships. Governing equations are given for the key variables which are, in the present case, (1) the refining agent concentration, (2) the gas species dissolved in the liquid phase, and (3) the bubble radius, gas molar fraction, and density function. The method of solution based on the backward method of characteristics is briefly discussed.

1. Introduction

The quality of glass products is degraded if gas bubbles and unfused silica grains remain in the molten glass as it is being pulled from the furnace [1,2]. Having fewer defects, especially fewer remaining bubbles, has become a major requirement in the new quality standards for many commercial glass products. For example, in TV-glass production, a presence of six bubbles per ton of glass results in 10% rejection rate of the final product, and for new products such as High Definition Television, the quality requirements are even more stringent [3]. For automotive window glass, the most demanding specification requires that gas bubbles be less than 0.5 mm in diameter for transparency purposes [4]. Moreover, for automobile windshield glass, reducing by half the defect density would increase the profitability by more than 2 millions dollars per year per plant [4].

Radiation is the main mode of heat transfer in glass melting furnaces. As shown by Pilon and co-workers [5–7] even a small number of entrapped bubbles can affect the radiation characteristics of semitransparent media provided that the bubble radius is much larger than the wavelength of radiation and that the medium is weakly absorbing. Moreover, these bubbles may accumulate or rise to the free liquid surface and form a foam layer which has significant negative effects on the energy efficiency, the glass quality, the productivity, the pollutant emissions, and the furnace integrity [8].

The goal of the present work is to develop a general model for bubble transport, growth and shrinkage in three-dimensional flows. The flow is assumed to be laminar for the sake of simplicity. The bubbles can grow or shrink due to diffusion of gases in and out of the bubbles. The analysis presented is as general as possible and can find applications in many materials processing situations for at least one of the following reasons: (1) for predicting the radiation transfer in liquid containing bubbles, (2) for predicting the foam formation, and/or (3) for improving the quality of manufactured products. Applications to glass melting furnaces appear to be the most natural one since glass is one of the most common

* Corresponding author. Tel.: +1-310 206 5598; fax: +1-310 206 4830.
E-mail address: pilon@seas.ucla.edu (L. Pilon).

0022-3093/$ - see front matter © 2004 Elsevier B.V. All rights reserved.
doi:10.1016/j.jnoncrysol.2004.01.010

Nomenclature

A	frequency factor in Arrhenius equation
C	mass concentration
D	diffusion coefficient
$D_{\text{eff}}\|_{\text{f}}$	effective diffusion coefficient of the foam layer
E	activation energy
f	fugacity
f_1	bubble density function
g	specific gravity
h	bubble generation rate per unit volume in the state space
H_∞	steady-state foam thickness
$\vec{i},\vec{j},\vec{k}$	unit vectors in the physical space
j,k	oxidation indices of the refining agent
$j(x,y)$	superficial gas velocity at the glassmelt surface
k_{r}	refining reaction rate constant
K	mass transfer coefficient
l	number of gas species diffusing into and out of the bubbles
$\dot{m}$	mass flux
M	refining agent ion
M_i	molecular mass of gas species 'i'
$\overline{M}$	mean molecular mass
p	pressure
p_i	partial pressure of gas species 'i'
q	order of the refining reaction
r	bubble radius
R	universal gas constant = 8.314 J/mol K
S	solubility of the gas species in the molten glass
T	temperature
t	time
u	projection of the velocity vector on the x-axis
v	projection of the velocity vector on the y-axis
V	volume
$\vec{v}$	velocity vector
w	projection of the velocity vector on the z-axis
w_{r}	vertical upward velocity of the bubble relative to the glassmelt
$\vec{x}$	spatial or external coordinates
x	longitudinal location (see Fig. 1)
y	spanwise location (see Fig. 1)
z	local depth within the glassmelt (see Fig. 1)

Greek symbols

α	parameter [Eq. (20)]
γ_i	molar fraction of gas species 'i' inside the bubble
σ	surface tension
ρ	density
μ	kinematic viscosity

Subscripts

b	refers to the bubbles
batch	refers to the batch
comb	refers to the combustion space
diff	refers to gas diffusion from the the glassmelt to the gas bubbles
e	equilibrium property at the bubble/glassmelt interface
i	index of the gas species
int	refers to the surface of the glassmelt
M	refers to the refining agent
n	index of the bubble group
O_2	refers to the oxygen
ref	refers to refining reaction
∞	refers to the bulk of the glassmelt

Notations

[X]	molar concentration of species X in the glassmelt
$\dot{\text{X}}$	derivative of property X with respect to time

and available semitransparent media that is weakly absorbing in the infrared spectral region from 0.2 to 4.5 μm [9,10].

1.1. General description of the glass melting process

Fig. 1 shows a schematic of a typical glass melting furnace. During the glass making process, the glass batch is introduced in the glass melting furnace where it spreads due to convection currents in the molten glass and melts due to the heating from the flames in the combustion space and/or from Joule heating in electric melters. Melting of raw batch materials is a complex physicochemical process which involves a large number of chemical reactions and phase transformations occurring over the wide temperature range from 800 to 1200 °C [11]. For example, in the typical container glass manufacturing the basic and most important reaction in the batch involve silica, sodium carbonate, and calcium carbonate [12],

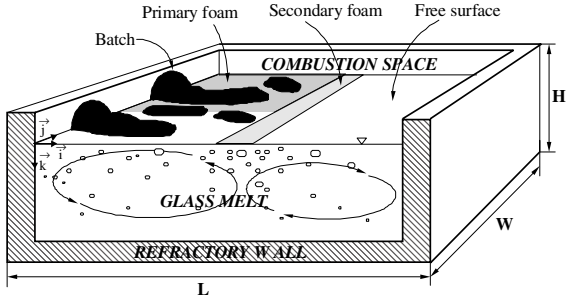

Fig. 1. Schematic of a glass melting furnace and the coordinate system.

$$CaCO_3 + Na_2CO_3 \rightarrow Na_2Ca(CO_3)_2 \quad \text{around } 550\ ^\circ\text{C}, \tag{1}$$

$$Na_2Ca(CO_3)_2 + 2SiO_2 \rightarrow Na_2O \cdot SiO_2 + CaO \cdot SiO_2 + 2CO_2 \quad 600\text{–}830\ ^\circ\text{C}, \tag{2}$$

$$Na_2CO_3 + SiO_2 \rightarrow Na_2 \cdot SiO_2 + CO_2 \quad 720\text{–}900\ ^\circ\text{C}, \tag{3}$$

$$2CaCO_3 + SiO_2 \rightarrow CaO \cdot SiO_2 + 2CO_2 \quad 600\text{–}900\ ^\circ\text{C}. \tag{4}$$

Carbon dioxide gas is produced as a result of the last three reactions and it mainly diffuses in the melt [1]. A small fraction of the gas contributes to heterogeneous nucleation of bubbles within or just below the batch. Some of these bubbles pass through the batch and reach the combustion space, while the others are trapped in the melt and are carried with the convection currents in the glass bath. Refining agents, which are involved in the equilibrium redox reactions producing or consuming gases, are usually added to the batch in order to remove undesirable bubbles from the glassmelt [1,13,14]. Three types of refining agents are commonly used [15]:

1. Variable-valence metal oxides which release only oxygen, e.g., the antimony oxide (Sb_2O_5/Sb_2O_3), the arsenic oxide (As_2O_5/As_2O_3), and the cesium oxide (CeO_3/CeO_2) [14,16–19].
2. Sulphates and sulphites which release a mixture of sulphur dioxide (SO_2) and oxygen [19]. For example, sodium sulphate (Na_2SO_4) is used as a refining agent at high temperatures (around 1800 °C) but it also accelerates the melt formation if introduced in suitable proportions [20]. However, a detailed explanation of the beneficial effects of sulphate is not yet available.
3. Chlorides, bromides, and iodines which evaporate at refining temperature [15].

The fusion of raw materials in the batch and the fining reactions taking place in the glassmelt generate a large number of gas bubbles. A fraction of these bubbles is entrapped on the free surface of the glass to produce the primary foam [12]. Resorption of the remaining small fining gas bubbles, taking place during the conditioning of the glassmelt as it flows from the hot spot in the middle towards the throat of the furnace, also leads to formation of the so-called secondary foam [12]. Visual observations and laboratory scale studies of furnace operations indicate that the foam layers of various thickness can cover a large fraction of the free surface of the molten glass [12,21].

1.2. Literature review

Previous studies of the bubble behavior in glassmelt were mainly concerned with individual bubbles in an infinitely large quiescent pool of molten glass at a uniform temperature. The simplest of such studies consists of studying the shrinkage or growth of a stationary bubble containing a single gas [22,23] sometimes accounting for refining reactions [16,17]. Other studies were concerned with a stationary bubble containing several gases with or without refining reactions [17,24,25]. More realistic situations were investigated by accounting for the bubble rise due to buoyancy for a single gas bubble [2,26] or a bubble containing several gases [27,28], including the presence of refining reactions [14,15,18]. All of these studies show that in the presence of refining agents, only two mechanisms are mainly responsible for the removal of gas bubbles from the melt. They are:

- First, in high temperature regions, the equilibrium of the refining reaction shifts to gas production [1]. Then, the fining gas produced diffuses from the molten glass into already existing gas bubbles. In addition, gases already contained in bubbles are being diluted by the incoming fining gas [1,29], and, in turn, this enhances the diffusion of gases from the melt into the growing bubbles. Diffusion of fining gases makes bubbles grow in size until the buoyancy force is large enough to enable them to rise to the glassmelt free surface.
- Second, at low temperatures, the equilibrium of the fining reaction shifts to gas consumption resulting in gas diffusion from the bubbles to the melt. Small bubbles, which did not yet grow to a sufficiently large size, then dissolve in the glassmelt [19]. However, recent studies [30,31] demonstrate that the refining reaction involving antimony oxide in TV panel glass was complete and irreversible, i.e., bubble shrinkage due to gas consumption at low temperatures was not clearly evident.

Even though modeling the behavior of individual bubbles gives an insight into the mechanism of bubble generation, growth, and shrinkage, it does not lead to any conclusions about the overall performance of the refining process. To accomplish the latter objective, one approach is to trace bubbles as they grow and shrink while being transported in the glass bath through regions of different temperatures, gas concentrations and pressures [1,13,29,30]. In this approach, bubbles are introduced at the batch/glassmelt interface and are followed individually. All the studies reported [1,13,29,30] assume that probabilistic events such as the bubble coalescence or breakage or bubble nucleation are negligible. Moreover, they neglected the interdependence of

gas concentration in the glassmelt and mass transfer in and out of the bubbles thus enabling them to solve successively (1) the glass flow and thermal structure, (2) the gas concentrations dissolved in the glassmelt, and (3) the trajectory and growth or shrinkage of a large number of individual single or multicomponent gas bubbles. The results are analyzed using statistical methods [1] in order to assess the degassing efficiency of a new tank design or new process conditions. The tracing method is a useful technique to elucidate the bubble trajectories in the molten glass. However, it is tedious to implement and does not provide detailed information about the number of bubbles and their size distribution at any given location throughout the tank. Therefore, the bubble-tracing approach cannot account for the coupling between the concentration of gases dissolved in the molten glass, the bubble density function, the growth rate, and the glass flow and temperature fields. In addition, it can hardly be used to predict foaming at the surface of the glassmelt.

An alternative approach has been proposed by Ungan et al. [32] that consists of solving the conservation equation for the total number of bubbles and taking into account the effect of bubbles on the flow and temperature fields of the molten glass through the reduction of the effective density of the two-phase mixture. However, only monodispersed bubbles with constant radius were considered and refining reactions and bubble growth due to pressure change and gas diffusion were neglected.

In contrast, the population balance theory [33] allows one to predict in detail the radius and gas content of polydispersed bubbles and their density function throughout the glass melter. The only attempts to employ population balance theory to the bubble dynamics in glass tanks are due to Roi et al. [34] and Balkanli and Ungan [35]. Roi et al. [34] proposed a two-dimensional model for calculating the time dependence of the bubble size distribution assuming that the bubble growth rate is independent of the bubble radius. However, the authors admitted that their model 'contains substantial simplifications and cannot be used for the exact quantitative modeling of concrete melting vessels'. Balkanli and Ungan [35] presented a more realistic study based on a discretized formulation of the three-dimensional steady-state population balance equation (PBE). However, the practical application of both works appear to be very limited since several highly simplifying assumptions have been made such as: (1) refining reactions are not considered, (2) bubble nucleation in the melt and at the refractory walls is neglected, (3) each gas bubble contains only one diffusing gas, and (4) the governing equations for the gas concentration in the molten glass, the bubble growth rate, and bubble population equation are solved independently, i.e., the coupling between these equations is neglected. Moreover, Balkanli and Ungan [35] solved the discretized form of the bubble population balance equation with a coarse grid in the bubble radius space. The limitations of these approaches have been discussed by Kumar and Ramkrishna [36]. In brief, the discrete formulation lacks of *internal consistency*, i.e., some of the moments of the bubble density function f_1 cannot be predicted accurately [36]. In other words, the calculation is designed for certain selected moments of the bubble density function rather than for an estimate of the bubble density function accurate enough for estimating all moments of the population [33,37].

The purpose of the present work is to propose a simplified yet realistic analysis of the bubble behavior in glass melting furnaces by using the population balance theory [33]. For the first time, it presents a complete set of coupled conservation equations for (i) the refining agent concentration, (ii) the concentrations of the gases dissolved in the glassmelt, and (iii) the bubble density function along with the associated boundary conditions and the closure laws. The model accounts for the three-dimensional convective transport of refining agent, gases, and bubbles as well as for bubble growth due to multiple gas diffusion and by taking into account bubble nucleation along the refractory walls and refining reactions. Finally, the method of characteristics and the associated numerical scheme used for solving the population balance equation in terms of the bubble density function f_1 are briefly described.

2. Physical model

The present analysis simplifies the mathematical formulation by decoupling the liquid and gas phase equations, i.e., the conservation equations for the liquid and gas phases are solved independently and the momentum and energy equations are solved only for the liquid phase assuming that no bubbles are present. Moreover, unlike previous studies [32,35,38] the study predicts the bubble density function f_1 of polydispersed bubbles and enables the accurate post-processing calculation of all the moments of the distribution.

2.1. Assumptions

In order to make the problem of bubble generation and transport in the glass melting tank mathematically tractable the following assumptions are made:

1. The effects of bubbles and dissolved gases on the velocity and on the temperature fields as well as on the thermophysical properties of the glassmelt are not considered.
2. Bubbles are perfectly spherical in shape. This assumption holds for air–molten glass flows at the pressures encountered in the glass melting tank.

3. The bubbles have negligible inertia ($\rho_b \ll \rho_\infty$). This hypothesis is reasonable since very small bubbles are present in the glass bath.
4. The components of the bubble velocity vector, are taken to be the same as those of the molten glass ($u_\infty, v_\infty, w_\infty$), except in the vertical direction where the buoyancy force has to be taken into account. In other words, the slip between the bubble and the glassmelt velocity is neglected except in the vertical direction. This can be justified by the fact that bubble are assumed to be small.
5. The molten glass is considered to be incompressible.
6. Local thermal equilibrium exists between the gas and liquid phases, i.e., $T_\infty = T_b = T$.
7. Coalescence and break-up of bubbles are not considered.
8. The gases in a bubble are perfectly mixed, and the gas mixture inside the bubbles behave as an ideal gas.
9. The bubbles are assumed to contain l different gas species.
10. The diffusing gas species 'i' is weakly soluble in the condensed phase (i.e., the Henry's law is applicable at the bubble/glassmelt interface).
11. The pressure in the bubbles remains close to the atmospheric pressure (maximum 5 atm [39]) so that the ideal gas approximation for fugacity is valid.
12. The diffusing gases neither react with the condensed phase nor undergo dissociation or association.
13. Neither chemical reactions between gases inside a bubble nor dissociation of gas molecules are taken into account.
14. The equilibration kinetics at the bubble surface are assumed to be very rapid, so that the rate limiting process is diffusion of gases in the melt.
15. The analysis presented is restricted to fining reactions that involve variable-valence metal oxides and produce oxygen only (in particular, the antimony oxide Sb_2O_5).

The above assumptions are commonly used in the treatment of bubble transport in three-dimensional laminar gravity-driven flow of molten glass [13,29–31,35]. Assumptions regarding the bubble velocity and neglect of the effects of bubbles on the liquid phase flow and temperature fields are the most severe one and their limitations will be discussed later. They have been used to decouple the conservation, momentum, and energy equations of the liquid and gas phases. This approach can be justified by the facts that bubble radius and concentration are small and that the alternative approach solving the coupled governing equations using the two-fluid model lacks mechanistic closure laws accounting, for example, for the interfacial momentum transfer [40]. Moreover, the effect of bubbles on the thermophysical properties of the glassmelt such as the dynamic viscosity, the thermal conductivity, and the specific heat are not clearly known. This is particularly true for the effect of bubbles on the radiation characteristics of molten glass that have been addressed in Refs. [5–7].

2.2. Refining agent concentration in the glassmelt

2.2.1. Refining reaction

As mentioned in the Introduction, the refining agent is introduced into the melting tank as part of the batch. As the agent is carried by the flow of the molten glass and encounters high temperature regions, the following reversible chemical reaction for variable-valence metal oxides, written in a generalized form, takes place [41]:

$$\mathrm{M}^{k+} + \frac{k-j}{2}\mathrm{O}^{2-} \rightleftharpoons \frac{k-j}{4}\mathrm{O}_2 + \mathrm{M}^{j+}. \tag{5}$$

In the case of antimony oxide as a refining agent, Kawachi and Kawase [13,30] and Kawachi and Kato [31] showed that the rate of the backward reaction can be neglected in the production of TV panel glass. Therefore, the refining reaction can be considered as irreversible with only the decomposition of the refining agent taking place. By assuming a constant oxygen ion activity and by defining q as the order of the refining reaction occurring at constant volume, the rate of the decomposition reaction can be expressed as [13,31]

$$-\frac{\partial[\mathrm{M}^{k+}]}{\partial t} = \left(\frac{k-j}{4}\right)\frac{\partial[\mathrm{O}_2]}{\partial t} = k_r[\mathrm{M}^{k+}]^q, \tag{6}$$

where the reaction rate constant k_r is calculated from the Arrhenius' law [30,31],

$$k_r = A\exp\left(-\frac{E}{RT}\right). \tag{7}$$

The pre-exponential parameter A and the activation energy E are constants determined experimentally.

2.2.2. Fining agent concentration

As follows from Eq. (6), the oxygen generation rate depends on the concentration of the dissociated form of the refining agent M^{k+}. Therefore, the local refining agent concentration $[\mathrm{M}^{k+}]$ is required in order to predict the transport of oxygen dissolved in the glass bath as well as the bubble generation rate. The species conservation equation for the refining agent in the glassmelt is given by

$$\frac{\partial[\mathrm{M}^{k+}]}{\partial t} + \nabla\cdot(\vec{v}_\infty[\mathrm{M}^{k+}]) = \nabla\cdot\left(D_\mathrm{M}\nabla[\mathrm{M}^{k+}]\right) - k_r[\mathrm{M}^{k+}]^q, \tag{8}$$

where $[\mathrm{M}^{k+}]$ is the molar concentration of metal ions and $\vec{v}_\infty$ is the local glassmelt velocity vector. The first term on the right-hand side of Eq. (8) accounts for the metal ion diffusion through the melt, while the last term represents the mass sink due to consumption of ions

M^{k+} by the refining reaction. Although the steady-state solution of the problem is sought, the transient term $(\partial[M^{k+}]/\partial t)$ has been retained for performing iterative numerical integration which results in the steady-state solution of the molar concentration $[M^{k+}]$.

2.2.3. Boundary conditions

Eq. (8) can be solved provided that boundary conditions are defined. The batch consists of the raw materials and cullet mixed with the refining agent in the form of oxides such as Sb_2O_5. The dissociation of the oxide occurs as the temperature increases leading to production of cations and anions such as M^{k+} and O^{2-}, respectively. Furthermore, assuming that the concentration of the refining agent is uniform within the batch, and the dissociation reaction at the batch/hot molten glass interface is instantaneous, complete, and irreversible, the concentration of the cations $[M^{k+}]$ should be constant everywhere at the batch/glassmelt interface:

$$[M^{k+}] = \text{constant} \quad \text{at the batch/glassmelt interface.} \tag{9}$$

The specific value of $[M^{k+}]$ depends on the process and the type of glass produced; it can be determined from operating data. Typically, antimony oxide is added in 0.1–1.0 wt% [19].

Finally, the gradient of the concentration $[M^{k+}]$ is taken to vanish at the glass/refractory walls and at the free surface of the molten glass

$$\nabla_{\vec{n}}[M^{k+}] = \vec{0} \quad \text{at the glassmelt/refractories interface,} \tag{10}$$

$$\nabla_{\vec{n}}[M^{k+}] = \vec{0} \quad \text{at the glassmelt/combustion space interface.} \tag{11}$$

Such boundary conditions can be justified by the fact that the diffusion of the cations from the glassmelt to the refractory walls and to the combustion space is negligible.

2.3. Dissolved gas transport in the glassmelt

The growth and shrinkage of the bubbles is, in part, caused by gas diffusion into and out of the bubbles due to a difference in concentration of a given gas species between the glassmelt and the gas bubbles. Therefore, one needs to predict the local concentration of each gas species dissolved in the glassmelt.

2.3.1. Species concentration equation

The transport of major gas species (O_2, H_2O, CO_2, and N_2) in the glassmelt is governed by the following general species concentration equation [13,42,43],

$$\frac{\partial C_{\infty,i}}{\partial t} + \nabla \cdot (\vec{v}_\infty C_{\infty,i}) = \nabla \cdot (D_i \nabla C_{\infty,i}) + \dot{m}_{\text{ref},i} - \dot{m}_{\text{diff},i}. \tag{12}$$

Here, $C_{\infty,i}$ and D_i are the mass concentration and the diffusion coefficient of the dissolved gas species 'i' in the glassmelt, respectively. The first term on the right-hand side of Eq. (12) accounts for mass diffusion of the dissolved gas species 'i' in the glassmelt. The source term $\dot{m}_{\text{ref},i}$ is the volumetric gas production rate due to the refining reaction, and the sink term $\dot{m}_{\text{diff},i}$ accounts for the volumetric diffusion rate of gas species 'i' from the glassmelt into the bubbles. As before, the transient term $[\partial C_{\infty,i}/\partial t]$ has been retained to enable iterative numerical integration of Eq. (12). Note that the last two terms on the right-hand side of Eq. (12) have been neglected by Balkanli and Ungan [42], while Kawachi and Kawase [13] neglected only the last term.

As stated in assumption 2, the analysis presented here is restricted to refining reactions that are complete and irreversible and produce oxygen only. Then, the source term $\dot{m}_{\text{ref},i}$ vanishes in the case of all gas species but oxygen. Solving Eq. (8) for $[M^{k+}]$ enables one to compute the oxygen generation rate per unit volume of glassmelt at every location in the glassmelt since

$$k_r[M^{k+}]^q = \left(\frac{4}{k-j}\right)\frac{1}{M_{O_2}}\frac{\partial C_{\infty,O_2}}{\partial t} = \left(\frac{4}{k-j}\right)\frac{\dot{m}_{\text{ref},O_2}}{M_{O_2}}. \tag{13}$$

After some rearrangement,

$$\dot{m}_{\text{ref},O_2} = \left(\frac{k-j}{4}\right) M_{O_2} k_r [M^{k+}]^q. \tag{14}$$

The sink term $\dot{m}_{\text{diff},i}$ is the total mass of dissolved gas species 'i' diffusing from the glassmelt into the bubbles per unit volume of the glassmelt and per unit of time at location $\vec{x}$ and instant of time t. It is given by

$$\dot{m}_{\text{diff},i}(\vec{x},t) = \int_0^1 \cdots \int_0^1 \left[\int_0^\infty K_i(C_{\infty,i} - C_{e,i}) f_1 \, dr\right] d\gamma_{i,1} \cdots d\gamma_{i,l-1}, \tag{15}$$

where $K_i(C_{\infty,i} - C_{e,i})$ is the total mass flow rate of the gas species 'i' from the glassmelt across the surface of a bubble of radius r expressed in [kg/s/bubble]. The concentration difference of gas species 'i' between the glassmelt and the bubble/glassmelt interface is $(C_{\infty,i} - C_{e,i})$. The bubble density function, i.e., the number of bubbles per unit volume at location $\vec{x}$ and time t having equivalent radii that lie within the range r to $r + dr$, and the molar fraction of gas species 'i' ranges between γ_i and $\gamma_i + d\gamma_i$ with $1 \leqslant i \leqslant l-1$ is denoted $f_1 = f_1[\vec{x}, r, t, (\gamma_i)_{1 \leqslant i \leqslant l-1}]$. Note that all the molar fractions of gas species 'i' γ_i sum up to unity. Thus, γ_l can be expressed as

a function of the remaining $(l-1)$ others and cannot be treated as an independent variable. When $C_{\infty,i} > C_{e,i}$ the gas species 'i' diffuses from the glassmelt in the bubbles, whereas when $C_{\infty,i} < C_{e,i}$ it diffuses from the gas bubbles to the glassmelt. Then, $\dot{m}_{\text{diff},i}(\vec{x},t)$ behaves either as a sink (if $C_{\infty,i} > C_{e,i}$) or as a source (if $C_{\infty,i} < C_{e,i}$). To complete the formulation, the closure laws must be specified as well as the boundary conditions.

2.3.2. Closure laws

To make the problem well-posed, the total mass flow of the gas species from the glassmelt to the bubbles and particularly the mass transfer coefficient K_i, and the gas concentrations at the bubble glassmelt interface, $C_{e,i}$, should be defined.

According to Levich [44], for bubbles moving at low relative velocities w_r (Reynolds number much smaller than unity) in a quiescent liquid containing diffusing gases, the coefficient K_i can be expressed as

$$K_i = 7.98 D_i^{2/3} w_r^{1/3} r^{4/3} \quad (\text{in } \text{m}^3/\text{s}). \tag{16}$$

Here, D_i is the diffusion coefficient of gas species 'i' in the glassmelt while w_r is the relative velocity of the bubble of radius r with respect to the liquid. Extensive studies have shown that in molten glass small bubbles behave like solid sphere while large spherical bubbles behave like fluid spheres (see Ref. [19] for an in-depth review). According to the Stokes' law for solid spheres, the small gas bubbles rise in the molten glass with the relative vertical velocity given by

$$w_r = \frac{2}{9}\frac{\rho_\infty g r^2}{\mu_\infty}. \tag{17}$$

On the other hand, in the case of large spherical bubbles in the molten glass, the vertical velocity relative to the molten glass follows the Hadamar–Rybczynski formula [19,45]:

$$w_r = \frac{1}{3}\frac{\rho_\infty g r^2}{\mu_\infty}. \tag{18}$$

Unfortunately, there are no clear criteria regarding what bubbles should be considered as large or small. Experimental results suggested that bubbles of diameter larger than 1 mm can be considered as large and their velocity follows Eq. (18) [45]. In brief, the bubble rise velocity with respect to liquid phase can be written as

$$w_r = \alpha\frac{\rho_\infty g r^2}{\mu_\infty}, \tag{19}$$

where α is a parameter that depends on the bubble size according to Eqs. (17) and (18):

$$\alpha = \begin{cases} 2/9 & \text{for small bubbles } (2r \leqslant 1 \text{ mm}), \\ 1/3 & \text{for large bubbles } (2r \geqslant 1 \text{ mm}). \end{cases} \tag{20}$$

Note that Eqs. (17)–(19) correspond to the terminal (i.e., steady-state) velocity of spherical bubbles, i.e., the transient motion of bubbles have not been considered for the sake of simplicity and since its formulation is still incomplete and quite involved [46].

In the present analysis, the magnitude of the mass flux is assumed to be relatively small, so that the variations of mass concentration of gas species 'i' in both phases are small as well. Then, the local quasi-equilibrium can be assumed to exist at the bubble/molten glass interface [47], which implies the equality of the chemical potentials of the diffusing gas on both sides of the interface. This fact, combined with assumptions 3, 8 and 10, allows us to apply the generalized Henry's law and obtain the relationship between species concentrations on both sides of the bubble/glassmelt interface [48],

$$C_{e,i} = S_i M_i f_{b,i}. \tag{21}$$

Here, $C_{e,i}$ is the concentration of the diffusing gas 'i' at the interface (assumed to be at equilibrium) and S_i is the solubility of gas species 'i' in the glass melt, M_i is the molecular weight of the species 'i', and $f_{b,i}$ the fugacity of the species 'i' in the bubble. Provided that the pressure is low enough and the ideal gas approximation holds (assumption 9), the fugacity $f_{b,i}$ is approximately equal to the partial pressure of species 'i' ($p_{b,i}$) on the gas side of the interface [39], so that

$$C_{e,i} = S_i M_i p_{b,i}. \tag{22}$$

Using an ideal gas equation of state (assumption 7), the partial pressure of the gas species 'i' in the bubble is given by the Raoult's law:

$$p_{b,i} = \gamma_i p_b, \tag{23}$$

where γ_i is the molar fraction of gas species 'i' inside the bubble and is such that

$$\sum_{i=1}^{l} \gamma_i = 1. \tag{24}$$

This results in the following jump condition for the species concentrations at the bubble/glassmelt interface:

$$C_{e,i} = \gamma_i S_i M_i p_b. \tag{25}$$

2.3.3. Boundary conditions

According to Balkanli and Ungan [35], the concentration of carbon dioxide (CO_2) at the batch/glassmelt interface can be taken as being the saturation concentration owing to the very high intensity of gas generation due to fusion and melting of the raw batch materials. Also, as speculated by Kawachi and Kawase [13], oxygen (O_2) is supplied in sufficiently large amounts from the combustion space or by refining reactions taking place in the batch to saturate the glassmelt beneath the batch/glassmelt interface; similarly, for nitrogen (N_2) in air fired furnaces. However, transport of nitrogen can be neglected in oxy-fired furnaces since it is present in very small amount.

At the glass/refractory wall interface, the gradient of the concentration of gas species 'i' in the glassmelt is assumed to vanish owing to the absence of mass transfer through the refractory walls:

$$\nabla_{\vec{n}} C_{\infty,i} = \vec{0} \quad \text{at the glassmelt/refractories interface.} \tag{26}$$

In cases when the free surface of the glassmelt is in direct contact with the combustion gases, the gas concentration at the free surface is given by the Henry's law [13,31,42], i.e.,

$$C_{\infty,i} = S_i M_i p_i|_{\text{int}}$$
at the glassmelt/combustion space interface, (27)

where $p_i|_{\text{int}}$ is a partial pressure of gas species 'i' on the combustion side of the glassmelt/combustion space interface and is obtained from the calculation of the gas species concentrations as well as the flow and temperature fields in the combustion space.

However, if the free surface is covered by a foam blanket then the effect of foam should be accounted for by equating the mass fluxes on both sides of the foam/glassmelt interface, i.e.,

$$D_i(\nabla C_{\infty,i}) = D_{\text{eff}}|_{\text{f},i} \nabla(C_{\infty,i})$$
at the glassmelt/foam interface, (28)

where $D_{\text{eff}}|_{\text{f},i}$ is the effective diffusion coefficient of gas species 'i' through the foam layer and $C_i|_{\text{int}}$ is the gas concentration at the foam/glassmelt interface. The left-hand side of Eq. (28) represents the gas diffusion mass flux on the glass side, while the right-hand side represents that on the foam side. Assuming that the foam thickness is small, a linear approximation of the gas concentration in the foam layer yields the following mixed boundary condition,

$$D_i \nabla C_{\infty,i} = D_{\text{eff}}|_{\text{f},i} \left(\frac{C_i|_{\text{comb}} - C_{\infty,i}}{H_\infty} \right)$$
at the glassmelt/foam interface, (29)

where H_∞ is the steady-state foam thickness (see Ref. [49]) and $C_i|_{\text{comb}}$ the gas concentration at the foam/combustion space interface, i.e., at the top of the foam layer. A model for the effective diffusion coefficient of gas species 'i' through the foam layer, $D_{\text{eff}}|_{\text{f},i}$ can be found in the literature [50].

2.4. Bubble density population

2.4.1. Single bubble environment

A schematic of a single bubble in mechanical and thermal equilibrium with the surrounding molten glass is given in Fig. 2, along with the corresponding p–T diagram. The Young–Laplace equation relates the pressure (p_b) inside a spherical bubble of radius r with

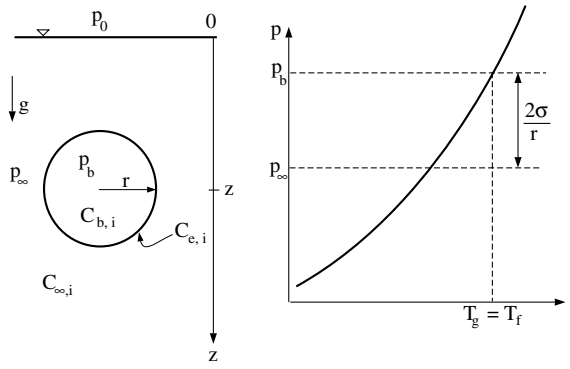

Fig. 2. Schematic of a single bubble in thermal equilibrium with the glassmelt and the corresponding p–T diagram.

the pressure (p_∞) in the surrounding glassmelt and the surface tension σ by

$$p_b = p_\infty + \frac{2\sigma}{r}. \tag{30}$$

Since the velocity of the viscous molten glass in the glass bath is very small (of the order of 1 cm/s) the pressure field in the tank can be assumed to be purely hydrostatic. Thus, the total pressure inside the bubble is expressed as

$$p_b = p_0 + \rho_\infty g z + \frac{2\sigma}{r}, \tag{31}$$

where p_0 is the pressure at the free surface of the molten glass and z is the local depth within the glassmelt.

Based on assumption 5, the components of the bubble velocity vector $\vec{v}_b$ can be expressed as

$$\vec{v}_b(\vec{x}) = u_\infty \vec{i} + v_\infty \vec{j} + (w_\infty - w_r)\vec{k} \tag{32}$$

with w_r being the upward bubble velocity relative to the molten glass due to the buoyancy force given by Eq. (19). Note that according to our convention, the vertical axis is oriented downward. Values of u_∞, v_∞, and w_∞, are obtained from the thermal-flow computation of molten glass circulation in the bath (see, for example, Refs. [51–55]).

2.4.2. Bubble population balance equation

As discussed in detail by Ramkrishna [33,56], the bubble population can be described by a state vector defined in a so-called state space. Each bubble in the glassmelt is characterized by its radius r and the molar fraction of gas species 'i' contained in the bubble γ_i. Let $f_1[\vec{x}, t, r, (\gamma_i)_{1 \leqslant i \leqslant l-1}]$ be the average number density function of bubbles. As already discussed, γ_l cannot be treated as an independent variable. The average number density function $f_1[\vec{x}, t, r, (\gamma_i)_{1 \leqslant i \leqslant l-1}]$ is assumed to be sufficiently smooth to allow differentiation with respect to any of its variables as many times as necessary [33]. Note that the temperature of the bubbles is assumed to be the same as that of the glassmelt, i.e., the local

thermal equilibrium prevails. Therefore, although the temperature is important to determining the growth rate of a bubble, it is a continuous phase (glassmelt) variable and hence does not enter the characterization of the bubble state. Considering the bubbles generated and transported by the flow of the glassmelt, and assuming that there are l gases diffusing into or out of each bubble, the state vector $\vec{S}$ can be expressed as $\vec{S} = [x, y, z, t, r, (\gamma_i)_{1 \leqslant i \leqslant l-1}]$. Then, the population balance equation can be expressed as

$$\frac{\partial f_1}{\partial t} + \frac{\partial}{\partial x}(u_\infty f_1) + \frac{\partial}{\partial y}(v_\infty f_1) + \frac{\partial}{\partial z}[(w_\infty - w_r) f_1] + \frac{\partial}{\partial r}(\dot{r} f_1) + \sum_{i=1}^{l-1} \frac{\partial}{\partial \gamma_i}(\dot{\gamma}_i f_1) = h, \tag{33}$$

where w_r is given by Eq. (19). The time rate of change of the bubble radius and of the molar fraction of gas species 'i' inside the bubble are denoted by $\dot{r}$ and $\dot{\gamma}_i$, respectively. The transient term $\partial f_1/\partial t$ represents the time rate of change of the bubble density, and the other two terms on the left-hand side of Eq. (33) represent advection of the bubble density function in the physical space and in the property space, respectively. Finally, the term h represents the net rate of production of bubbles of a particular state $(\vec{x}, r, (\gamma_i)_{1 \leqslant i \leqslant l-1})$ at time t.

The molar fraction of gas species 'i' can be expressed as a function of the mass concentrations $C_{b,i}$ since by definition

$$\gamma_i = \frac{C_{b,i}/M_i}{\sum_{j=1}^{l}(C_{b,j}/M_j)} = \frac{C_{b,i} RT}{M_i p_b}. \tag{34}$$

Then, the time derivative of the molar fraction of gas species 'i' in the bubble γ_i can be expressed as

$$\dot{\gamma}_i = \gamma_i \left[\frac{\dot{C}_{b,i}}{C_{b,i}} - \frac{\rho_\infty g (w_\infty - w_r) - 2\sigma \dot{r}/r^2}{p_b} \right], \tag{35}$$

where $C_{b,i}$ and $C_{\infty,i}$ are the mass concentrations of gas species 'i' in the bubble and in the glassmelt, respectively. Eq. (36) indicates that if a bubble contains a single gas, the bubble can only shrink since the concentration of gas dissolved in the glassmelt $C_{\infty,i}$ (in kg/m^3) cannot be larger than the gas solubility given by $S_i M_i (p_0 + \rho_\infty g z)$. Substituting the expression for K_i given by Eq. (16) and that of $C_{e,i}$ given by Eq. (25) and differentiating the left-hand side of Eq. (36) yields

$$\frac{4\pi}{3} r^3 \dot{C}_{b,i} + C_{b,i} 4\pi r^2 \dot{r} = 7.98 (C_{\infty,i} - \gamma_i S_i M_i p_b) D_i^{2/3} w_r^{1/3} r^{4/3}. \tag{37}$$

Then, solving for $\dot{C}_{b,i}$ results in

$$\dot{C}_{b,i} = \frac{1.905}{r} \left(\frac{\alpha \rho_\infty g D_i^2}{\mu_\infty} \right)^{1/3} (C_{\infty,i} - \gamma_i S_i M_i p_b) - \frac{3\dot{r}}{r} C_{b,i}. \tag{38}$$

According to the Dalton's law for ideal gases, the total pressure of the gas mixture in the bubble is given by

$$p_b = \sum_{i=1}^{l} (p_{b,i}) = \left[\sum_{i=1}^{l} \left(\frac{C_{b,i}}{M_i} \right) \right] RT. \tag{39}$$

The derivative of Eq. (39) with respect to the time t using the expression for $\dot{C}_{b,i}$ given by Eq. (38) results in

$$\frac{\partial p_b}{\partial t} = \frac{1.905 RT}{r} \left(\frac{\alpha \rho_\infty g}{\mu_\infty} \right)^{1/3} \times \sum_{i=1}^{l} \frac{D_i^{2/3}}{M_i} [(C_{\infty,i} - \gamma_i S_i M_i p_b)] - \frac{3\dot{r}}{r} p_b. \tag{40}$$

The temperature T is obtained from the steady-state solution of the thermal-flow calculations of the glassmelt. Substituting the expression for p_b given by Eq. (31) into Eq. (40), assuming that $\partial p_0/\partial t = 0$ (steady-state), and solving for the growth rate $\dot{r}$ gives

$$\dot{r} = \frac{0.635 RT \left(\frac{\alpha \rho_\infty g}{\mu_\infty} \right)^{1/3} \sum_{i=1}^{l} \left[\frac{D_i^{2/3}}{M_i} (C_{\infty,i} - \gamma_i S_i M_i p_b) \right] - \rho_\infty g (w_\infty - w_r) r/3}{p_0 + \rho_\infty g z + 4\sigma/3r}. \tag{41}$$

where $\dot{r}$ and $\dot{C}_{b,i}$ are the time rate of change of the bubble radius and of the mass concentration of gas species 'i' contained in the bubbles, respectively. Expressions for $\dot{r}$ and $\dot{C}_{b,i}$ can be derived from assumptions 8 to 10 by writing the time rate of change of the mass of gas species 'i' contained in a spherical bubble of radius r as [44]

$$\frac{dm_i}{dt} = \frac{d(C_{b,i} V_b)}{dt} = K_i (C_{\infty,i} - \gamma_i S_i M_i p_b), \tag{36}$$

The first term in the numerator of Eq. (41) takes into account the change of radius due to mass transfer at the bubble interface, while the second term accounts for the change in pressure as the bubbles are transported in the glass bath. Such an expression has been previously derived by Balkanli and Ungan [2], but the expression for the term accounting for growth due to the change in pressure appears to be in error as also confirmed by other studies for quiescent glassmelt ($w_\infty = 0$) [14,28].

Note that the gas and liquid momentum equations have been decoupled and it was assumed that the vertical component of the bubble velocity vector was given by $w_b = w_\infty - w_r$. It implies that the bubble velocity field does not satisfy the continuity equation in steady-state, i.e., $\nabla \cdot \vec{v}_b \neq 0$ [37]. Therefore, assumptions 2 and 5 introduce an artificial source in the population balance equation. In order to approximately conserve the total number of bubbles the bubble velocity vector $\vec{v}_b$ should satisfy

$$\nabla \cdot \vec{v}_b = \nabla \cdot \vec{v}_\infty - \frac{\partial w_r}{\partial z} \approx 0. \tag{42}$$

Since the molten glass is treated as incompressible, Eq. (42) is satisfied if $\partial w_r/\partial z \ll 1$. Physically, this corresponds to situation where the bubble growth rate and liquid velocity does not vary significantly along the bubble pathline during the time interval t and $t + dt$.

2.4.3. Bubble generation

Finally, heterogeneous nucleation can occur on the surface of undissolved sand grains or on refractory walls [1]. Nemec [57] observed in an experimental crucible under uniform temperature conditions that heterogeneous bubble nucleation occurs at the surface of undissolved sand grains only if refining agent is present while homogeneous bubble nucleation could never be observed. It indicates that bubble nucleation takes place if the glassmelt is supersaturated with refining gases, i.e., if the local gas concentration dissolved in the molten glass exceeds the solubility at the local temperature and pressure. Cable and Rasul [58] reported that heterogeneous bubble nucleation occurred at the surface of the refractory even at small supersaturations. Finally, Roi et al. [59] have discussed bubble generation and formation of a bubble curtain consisting of very small bubbles located close to the refractory walls. The authors attributed the formation of a bubble curtain to the combination of an unfavorable temperature distribution and bubble growth rate.

Moreover, solving the gas species concentration equation (Eq. (12)) for oxygen could possibly yield oxygen concentrations higher than solubility within the glass bath due to the source from the refining reactions. However, such cases are expected only in the refining section of the tank where the number of undissolved sand grains is predicted to be small [60], thus limiting the number of available nucleation sites. Instead, the main mechanism for dissolved oxygen removal from the glassmelt is the diffusion in already existing bubbles to make them grow and rise at the surface. Note also that from a thermodynamics point of view gas diffusion is favored over heterogeneous nucleation. Therefore, given the complexity of the physical phenomena and the controversy regarding the significance and mechanisms of heterogeneous nucleation in glass melting furnaces, heterogeneous nucleation has not been considered in the present study. The validity of this assumption will be examined in view of the numerical results presented in the second part of this document. Moreover, very fine grids close to the walls should be used to account for the entrainment by the flowing liquid of the very small bubbles generated at the refractory walls. Then, the grid size should be smaller than the typical size of a generated bubble making the calculation even more time consuming.

2.4.4. Boundary conditions

Boundary conditions for the bubble density function f_1 are required to solve the population balance equation (33) and are expressed as follows:

- *At the batch/glassmelt interface* bubbles exist in significant numbers due to the fusion/melting transformations taking place in the batch. The batch coverage is assumed to be known and the gas composition and the bubble density function are the same under the entire surface covered by the batch and does not vary with time. Then, the boundary condition at the batch/glassmelt interface is expressed as

$$f_1 = f_{1,0} \quad \text{at the glassmelt/batch interface,} \tag{43}$$

  where $f_{1,0} = f_{1,0}[r, (\gamma_i)_{1 \geqslant i \geqslant l-1}]$ is the bubble density function depending on the fusion/melting process and determined experimentally.
- *At the glassmelt/refractory wall interface* the boundary conditions appear to be controversial. Balkanli and Ungan [35], suggested the use of the weak boundary conditions at the refractory walls. However, Swarts [4] mentioned that the number of bubbles per unit volume generated at the glass/refractory interfaces is significant. Until further experimental results are obtained we will assume that the gradient of f_1 in the normal direction vanishes,

$$\nabla_{\vec{n}} f_1 = \vec{0} \quad \text{at the glassmelt/refractories interface.} \tag{44}$$

- *At the free surface of the glassmelt* Balkanli and Ungan [35] used the same boundary condition as that used at the glass/melt/refractory wall interface, i.e., $\nabla_{\vec{n}} f_1 = \vec{0}$. Physically, such a boundary condition means that no bubble can escape through the glassmelt free surface. Obviously, such a boundary condition does not represent the physical phenomena occurring since a single bubble reaching a free interface can either merge with the interface almost instantaneously or bounce back one or several times before stabilizing at the free interface to finally burst [61]. Additional complications appear when bubbles accumulate to form a foam layer at the glassmelt surface. Then, rising bubbles aggregate and coalescence with

bubbles in the foams. This phenomenon is suspected to be of major importance for onset of foaming. To the best of our knowledge, no boundary conditions for the bubble density function f_1 at the glassmelt free surface and at the glassmelt/foam interface accounting for the physical phenomena described above are available in the literature. Note that the finite-difference algorithm needs the definition of these boundary conditions. On the other hand, the method of characteristics used in the present study does not require specification of any boundary condition at the glass/combustion space interface.

The local superficial gas velocity $j(x,y)$ at the glassmelt surface can be computed from the bubble density function:

$$j(x,y) = \int_0^1 \cdots \int_0^1 \left(\int_0^\infty f_1[x,y,z=0,r,(\gamma_i)_{1 \geqslant i \geqslant l-1}] \times \left(\frac{4\pi r^3}{3}\right)(w_\infty - w_r)\,\mathrm{d}r \right) \mathrm{d}\gamma_1 \cdots \mathrm{d}\gamma_{l-1}. \quad (45)$$

Then, the transient and steady-state foam thickness can be predicted from the analysis by Pilon et al. [49,62] for liquid foams generated from viscous liquids. However, the spreading of the foam over the glassmelt surface is not accounted for. The foam layer strongly affects the radiation heat transfer from the combustion space to the glass bath and can significantly reduce the glassmelt temperature [8,55]. Model for radiation transfer through foam and combined conduction and radiation transfer have been proposed recently [8,63–66] and should be used to recompute the glassmelt flow and thermal structures. However, this task is beyond the scope of the present work, and the presence of a foam layer will not be considered further.

3. Method of solution of model equations

Fig. 3 shows the block diagram of essential steps in the procedure which is used to calculate the bubble transport in the glass melting furnace. Previous studies computed the dissolved gas concentration in the melt by neglecting the source term in Eq. (12) due to the diffusion of gases in and out of the bubbles [35] and assumed that bubbles contain only one gas species. This simplification reduces the number of independent variables and implies that the dissolved gas concentrations $C_{\infty,i}$, the bubble radius r, and the bubbles density function f_1 can be computed consecutively and independently. In this study, the variables $C_{\infty,i}$, r, γ_i, and f_1 are interdependent and determined iteratively until all the solutions are converged as shown in Fig. 3. Considering refining reactions that are complete and irreversible enables us to compute the refining agent concentration $[M^{k+}]$ independently.

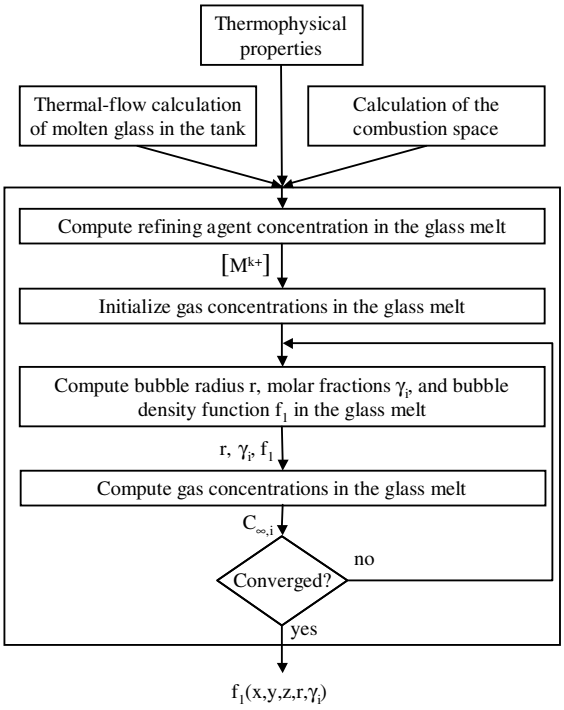

Fig. 3. Schematic lock diagram of the computational procedure.

The governing conservation equations and boundary conditions for the thermal-fluid calculations of the molten glass along with the numerical method of solution can be found elsewhere [51–54]. The governing partial differential equations for the refining agent concentration $[M^{k+}]$ and the gas concentrations $C_{\infty,i}$, are of parabolic type with the transient term included as an iteration parameter. For the purpose of numerical solution, the equations are discretized over the spatial coordinates by means of the control volume integration technique [66]. The resulting finite-difference approximation of derivatives produces a system of linear algebraic equations, which are then solved using line-by-line iterative method. The method solves a line of nodes by applying the tri-diagonal matrix inversion algorithm and sweeps the domain of integration in alternating directions along the coordinates axes. A fully implicit and unconditionally stable Euler method with very large time steps is employed to integrate the equations in time until steady-state solution is achieved. Numerical integration of the source/sink terms corresponding to gas diffusion in and out of the bubbles and given by Eq. (15) was performed using Simpson's rule for unequally spaced data. [1] The steady-state conditions for the refining agent concentration and the dissolved gas concentrations was assumed to be reached when the

[1] The Fortran subroutine is available at http://www.sali.freeservers.com/engineering/fortran_codes/unequal_simps. html.

residual for each of these variables was less than an arbitrary small value.

The population balance equation [Eq. (33)] is solved using the backward (or modified) method of characteristics described by Pilon and Viskanta [37]. In brief, the partial differential equation (33) is transformed into a system of ordinary differential equations by solving it along the characteristic curves in the particle state space defined as

$$\frac{\mathrm{d}x}{\mathrm{d}t} = u_\infty(x,y,z), \tag{46}$$

$$\frac{\mathrm{d}y}{\mathrm{d}t} = v_\infty(x,y,z), \tag{47}$$

$$\frac{\mathrm{d}z}{\mathrm{d}t} = w_\infty(x,y,z) - w_\mathrm{r}(x,y,z,r), \tag{48}$$

$$\frac{\mathrm{d}r}{\mathrm{d}t} = \dot{r}[x,y,z,,r,(\gamma_i)_{1\leqslant i\leqslant l-1},t], \tag{49}$$

$$\frac{\mathrm{d}\gamma_i}{\mathrm{d}t} = \dot{\gamma}_i[x,y,z,r,(\gamma_i)_{1\leqslant i\leqslant l-1},t] \quad \text{for } i=1,\ldots,l-1, \tag{50}$$

where w_r, $\dot{r}$, and $\dot{\gamma}_i$ are given by Eqs. (19), (41) and (35), respectively. If we assume that the liquid phase can be treated as incompressible, then, along the characteristic curves, the population balance equation (33) can be written as [37]

$$\frac{\mathrm{D}f_1}{\mathrm{D}t} = h + f_1\left[\frac{\partial w_\mathrm{r}}{\partial z} - \frac{\partial \dot{r}}{\partial r} - \sum_{i=1}^{l-1}\frac{\partial \dot{\gamma}_i}{\partial \gamma_i}\right], \tag{51}$$

where $\mathrm{D}f_1/\mathrm{D}t$ denotes the substantial derivative or the total time derivative along the pathline of the bubbles. The partial derivatives of w_r, $\dot{r}$, and $\dot{\gamma}_i$ with respect to z, r, and γ_i, respectively, are derived from Eqs. (19), (41) and (35) and expressed as

$$\frac{\partial w_\mathrm{r}}{\partial z} = \frac{2\alpha\rho_\infty g r\dot{r}}{\mu_\infty(w_\infty - w_\mathrm{r})} - \frac{\alpha\rho_\infty g r^2}{\mu_\infty^2}\frac{\partial \mu_\infty}{\partial z}, \tag{52}$$

$$\frac{\partial \dot{r}}{\partial r} = \frac{0.63RT\left(\frac{\alpha\rho_\infty g}{\mu_\infty}\right)^{1/3}\sum_{i=1}^{l}\left(2\sigma\gamma_i S_i D_i^{2/3}/r^2\right) - \frac{\rho_\infty g(w_\infty - 3w_\mathrm{r})}{3}}{p_0 + \rho_\infty g z + 4\sigma/3r} + \frac{4\sigma}{3r^2}\frac{\dot{r}}{p_0 + \rho_\infty g z + 4\sigma/3r}, \tag{53}$$

$$\frac{\partial \dot{\gamma}_i}{\partial \gamma_i} = -\frac{3\dot{r}}{r} - \frac{1.905 S_i RT}{r}\left(\frac{\alpha\rho_\infty g}{\mu_\infty}\right)^{1/3} \times\left[1 - \frac{\gamma_i(p_0 + \rho_\infty g z)}{p_0 + \rho_\infty g z + 4\sigma/3r}\right] - \frac{\rho_\infty g(w_\infty - w_\mathrm{r}) - 2\sigma\dot{r}/r^2}{p_\mathrm{b}}. \tag{54}$$

Eqs. (46)–(51) represent a system of ordinary differential equations that can be solved along the characteristic curves by the method of characteristics using inverse marching method with the same staggered grids as those used for computing the glassmelt velocity $\vec{v}_\infty$, temperature T, refining agent $[\mathrm{M}^{k+}]$, and dissolved gas concentrations $C_{\infty,i}$ fields enabling the coupling between all the variables. A detailed description of the numerical scheme has been presented by Pilon and Viskanta [37] and need not be repeated here.

The backward method of characteristics (or inverse marching method) is an interpretation of the Lagrangian approach that overcomes the difficulties related to mesh deformation. Based on a prespecified grid, it follows the particles backward in time as opposed to forward in the case of direct marching method. The backward method of characteristics uses a fixed grid that is also used for solving other transport equations such the momentum equation, the energy equation or the gas concentration in the continuous phase by finite-difference methods using a staggered grid as suggested by Patankar [66]. Thus, interactions between the particles or bubbles and the surrounding fluid can be easily accounted for in the numerical scheme. But unlike finite-difference methods that propagate the information along coordinate lines, the method of characteristics propagates the information along the pathlines and thus matches the physics of the flow resulting in accurate numerical results [37]. Other advantages of the method of characteristics are to overcome the numerical diffusion introduced by finite-difference methods [66] and to eliminate the need for outflow boundary conditions particularly at the glass free surface and glassmelt/foam interface. Moreover, the modified method of characteristics can be used for both transient and steady-state calculations with great accuracy and without problems of numerical instability.

4. Conclusion

This paper presented the mathematical formulation of bubble transport and generation in three-dimensional laminar gravity-driven flow. The mathematical model has been developed but is not limited to glass manufacturing and can be readily applied to other materials processing problems such as steel, aluminum, and polymers. After careful statement of the physical assumptions, the governing equations for (1) the refining agent concentration, (2) the gas species dissolved in the liquid phase, and (3) the bubble density function are derived. To the best of our knowledge, this study is the first one presenting a complete set of coupled governing equations for the key variables essential to assess the refining performances of a furnace. The method of solution and the convergence criteria are briefly discussed. The results will enable one to predict the quality of the glass, to simulate foaming of the glassmelt, and to determined the

number and size distribution of bubbles in the glassmelt which are critical for accurately predicting heat transfer from the combustion space to the glass bath [8,63,64]. The second part of this paper [67] presents the results of sample calculations.

Acknowledgements

This work was supported in part by the U.S. Department of Energy/Glass Industry/Argonne National Laboratory/University collaborative research project.

References

[1] R.G.C. Beerkens, Glastech. Ber. 71 (12) (1995) 369.
[2] B. Balkanli, A. Ungan, Glass Technol. 37 (1) (1996) 29.
[3] J.M Hermans, A.C. Verbeeks, Glastech. Ber. 67 (2) (1994) 49.
[4] E.L. Swarts, Glastech. Ber. 65 (4) (1992) 87.
[5] L. Pilon, R. Viskanta, J. Am. Ceram. Soc. 86 (8) (2003) 1313.
[6] D. Baillis, L. Pilon, F. Randranalisoa, R. Gomez, R. Viskanta, J. Opt. Soc. Am. A 21 (2004) 149.
[7] D. Baillis, F. Randranalisoa, L. Pilon, R. Viskanta, Identification of radiative characteristics of fused quartz containing bubbles using discrete ordinates method with Fresnel interfaces, in: Computational Thermal Radiation in Participating Media – EU-ROTHERM Seminar 73, Mons, Belgium, April 2003, p. 215.
[8] A.G. Fedorov, L. Pilon, J. Non-Cryst. Solids 311 (2002) 154.
[9] M. Rubin, Solar Energy Mater. 12 (1985) 275.
[10] C.Z. Tan, J. Arndt, J. Phys. Chem. Solids 62 (2001) 1087.
[11] A. Ungan, R. Viskanta, Glastech. Ber. 59 (10) (1986) 279.
[12] P.R. Laimbock, PhD thesis, Technical University of Eindhoven, Eindhoven, The Netherlands, 1998.
[13] S. Kawachi, Y. Kawase, Glastech. Ber. 71 (4) (1998) 83.
[14] E. Itoh, H. Yoshikawa, H. Miura, Y. Kawase, Glass Technol. 38 (4) (1997) 134.
[15] L. Nemec, Glass Technol. 21 (3) (1980) 134.
[16] R.G.C Beerkens, H. De Wall, J. Am. Ceram. Soc. 73 (7) (1990) 1857.
[17] H. Yoshikawa, Y. Kawase, Glastech. Ber. 70 (2) (1997) 31.
[18] H. Yoshikawa, H. Miura, Y. Kawase, J. Mater. Sci. 33 (10) (1998) 2701.
[19] J.E. Shelby, Handbook of Gas Diffusion in Solids and Melts, ASM International, Materials Park, OH, 1996.
[20] M. Cable, D. Martlew, Glass Technol. 37 (4) (1996) 137.
[21] J. Shell, Representative video and operating conditions of the Techneglas furnace C, personal communication, July 1999.
[22] M.C. Weinberg, P.I.K. Onorato, D.R. Uhlmann, J. Am. Ceram. Soc. 63 (1980) 175.
[23] L. Nemec, Glass Technol. 10 (1969) 176.
[24] M. Cable, J.R. Frade, Glastech. Ber. 60 (11) (1987) 355.
[25] M.C. Weinberg, P.I.K. Onorato, D.R. Uhlmann, J. Am. Ceram. Soc. 63 (1980) 435.
[26] P.I.K. Onorato, M.C. Weinberg, D.R. Uhlmann, J. Am. Ceram. Soc. 64 (1981) 676.
[27] E. Itoh, H. Yoshikawa, Y. Kawase, Glastech. Ber. 70 (1) (1997) 8.
[28] J.I. Ramos, J. Am. Ceram. Soc. 69 (2) (1986) 149.
[29] B. Balkanli, A. Ungan, Glass Technol. 37 (4) (1996) 137.
[30] S. Kawachi, Y. Kawase, Glastech. Ber. 71 (5) (1998) 111.
[31] S. Kawachi, M. Kato, Glastech. Ber. 72 (6) (1999) 182.
[32] A. Ungan, W.H. Turner, R. Viskanta, Glastech. Ber. 56K (1983) 125.
[33] D. Ramkrishna, Population Balances, Academic Press, San Diego, CA, 2000.
[34] O.T. Roi, G. Nölle Seidel, D. Höhne, Glastech. Ber. 67 (10) (1994) 263.
[35] B. Balkanli, A. Ungan, Glass Technol. 3 (5) (1996) 164.
[36] S. Kumar, D. Ramkrishna, Chem. Eng. Sci. 52 (4) (1997) 4659.
[37] L. Pilon, R. Viskanta, Int. J. Numer. Methods Fluids 42 (2003) 1211.
[38] P.M. Carrica, F.J. Bonetto, D.A. Drew, R.T. Lahey Jr., Int. J. Numer. Methods Fluids 28 (1998) 571.
[39] M.B. King, Phase Equilibrium in Mixtures, Pergamon, Oxford, 1969.
[40] R.T. Lahey, D.A. Drew, Chem. Eng. Commun. 118 (1992) 125.
[41] R. Pyare, S.P. Singh, A. Singh, P. Nath, Phys. Chem. Glasses 23 (5) (1982) 158.
[42] B. Balkanli, A. Ungan, Glass Technol. 37 (3) (1996) 101.
[43] J.-M. Rousseaux, C. Vial, H. Muhr, E. Plasari, Chem. Eng. Sci. 56 (2001) 1677.
[44] V.G. Levich, Physicochemical Hydrodynamics (translated from Russian), Prentice-Hall, Englewood Cliffs, NJ, 1962.
[45] E.M. Hornyak, M.C. Weinberg, Commun. Am. Ceram. Soc. 67 (11) (1984) C244.
[46] J.J.M. Magnaudet, The forces acting on bubbles and rigid particles, in: ASME Fluids Engineering Division Summer Meeting, FEDSM'97, Part 16, Vancouver, Canada, June 22–26, 1997, vol. 16, p. 1.
[47] R.B. Bird, W.E. Stewart, E.N. Lightfoot, Transport Phenomena, John Wiley, New York, 1960.
[48] I.M. Klotz, R.M. Rosenberg, Chemical Thermodynamics, Krieger, Malabar, FL, 1991.
[49] L. Pilon, A.G. Fedorov, R. Viskanta, J. Colloid Interf. Sci. 242 (2001) 425.
[50] L. Pilon, A.G. Fedorov, R. Viskanta, J. Cell. Plast. 36 (2000) 451.
[51] A. Ungan, R. Viskanta, Glastech. Ber. 60 (3) (1987) 71.
[52] A. Ungan, R. Viskanta, Glastech. Ber. 60 (4) (1987) 115.
[53] R. Viskanta, J. Non-Cryst. Solids 177 (1994) 347.
[54] L. Pilon, G. Zhao, R. Viskanta, Glass Sci. Technol. 75 (2) (2002) 55.
[55] L. Pilon, G. Zhao, R. Viskanta, Glass Sci. Technol. 75 (3) (2002) 115.
[56] D. Ramkrishna, Rev. Chem. Eng. 3 (1) (1985) 49.
[57] L. Nemec, J. Am. Ceram. Soc. 60 (9&10) (1977) 436.
[58] M. Cable, C.G. Rasul, J. Am. Ceram. Soc. 50 (10) (1967) 528.
[59] O.T. Roi, G. Nölle Seidel, D. Höhne, Glastech. Ber. 68 (7) (1995) 222.
[60] A. Ungan, R.U. Payli, B. Balkanli, J. Am. Ceram. Soc. 77 (7) (1994) 1921.
[61] R.D. Kirkpatrick, M.J. Lockett, Chem. Eng. Sci. 29 (1974) 2363.
[62] L. Pilon, A.G. Fedorov, R. Viskanta, Chem. Eng. Sci. 57 (2002) 977.
[63] A.G. Fedorov, R. Viskanta, Phys. Chem. Glasses 41 (3) (2000) 127.
[64] A.G. Fedorov, R. Viskanta, J. Am. Ceram. Soc. 83 (11) (2000) 2769.
[65] M. Varady, A.G. Fedorov, ASME J. Heat Transfer 124 (2002) 1103.
[66] S. Patankar, Numerical Heat Transfer and Fluid Flow, Hemisphere, Washington, DC, 1980.
[67] L. Pilon, R. Viskanta, J. Non-Cryst. Solids, this issue. doi:10.1016/j.jnoncrysol.2004.01.007.